



Facile Gold Nanorod Purification by Fractionated Precipitation

Journal:	<i>Nanoscale</i>
Manuscript ID:	NR-COM-03-2014-001592.R1
Article Type:	Communication
Date Submitted by the Author:	23-Apr-2014
Complete List of Authors:	Thai, Thibaut; Monash University , Materials Engineering; Melbourne Centre for Nanofabrication , Zheng, Yuanhui; Commonwealth Scientific and Industrial Research Organisation , Materials Science and Engineering; Melbourne Centre for Nanofabrication , Ng, Soon Hock; Monash University , Materials Engineering; Melbourne Centre for Nanofabrication , Ohshima, Hiroyuki; Tokyo University of Science, Faculty of Pharmaceutical Sciences Altissimo, Matteo; Melbourne Centre for Nanofabrication , Bach, Udo; Monash University, Department of Materials Engineering

COMMUNICATION

Facile Gold Nanorod Purification by Fractionated Precipitation

Cite this: DOI: 10.1039/x0xx00000x

T. Thai,^{a,c} Y. Zheng,^{b,c} SH. Ng,^{a,c} H. Ohshima,^d M. Altissimo^c and U. Bach^{a, b, c}

Received 00th January 2012,

Accepted 00th January 2012

DOI: 10.1039/x0xx00000x

www.rsc.org/

An efficient and facile size- and shape-selective separation of gold nanorod (GNR) solutions is developed using a fractionated precipitation strategy. This convenient method has the benefit of eliminating nanoparticulate side products that can substantially deteriorate the quality of self-assembled nanostructures. The fabrication of advanced plasmonic metamaterials crucially depends on the capacity to supply feedstocks of high-purity building blocks.

Metal nanoparticles and their assemblies possess unique electronic and optical properties.¹⁻³ The synthetic challenge is to produce these building blocks with monodisperse size and shape distributions. This is critically important for applications such as plasmonic waveguides where size and shape uniformity firstly affects the plasmonic coupling between neighboring metal nanoparticles and secondly the ability to produce defect-free arrays of these building blocks via self-assembly. A polydispersity in size and shape makes the collective optical response of nanoparticle assemblies complex and problematic to control. Furthermore, structural defects in nanoparticle waveguides have been shown to cause a strong damping in energy transport.⁴ Gold nanorods (GNRs) are of particular interest for plasmonic waveguiding.^{5,6} The ability to highly tune the wavelength at which their plasmonic resonances occur makes them attractive building blocks.⁷ The localized surface plasmons of GNRs can be excited in two modes following the long or the short axes referred as longitudinal and transverse modes respectively. Their anisotropic shape provides a rich diversity of plasmonic coupling regimes as a function of light polarization and their respective arrangement.^{8,9}

The most common method to produce GNRs is the seed-mediated synthesis that provides good control over the particle aspect ratio and size distribution.¹⁰ Unfortunately, a number of reaction byproducts are inevitably formed during this synthesis. In a

typical seed-mediated synthesis that yields GNRs with an aspect ratio of 3 and an average rod diameter of 15 nm (Fig. 1a), three typical byproducts are formed (Fig. 1b-d): large spheres with a diameter of 50 nm, square-shaped nanoplates with a width of 30 nm and a height of 25 nm (ESI, Fig. S1†) and high aspect ratio nanorods with smaller diameters. The diversity of the present byproducts makes the purification of GNR solutions particularly challenging.

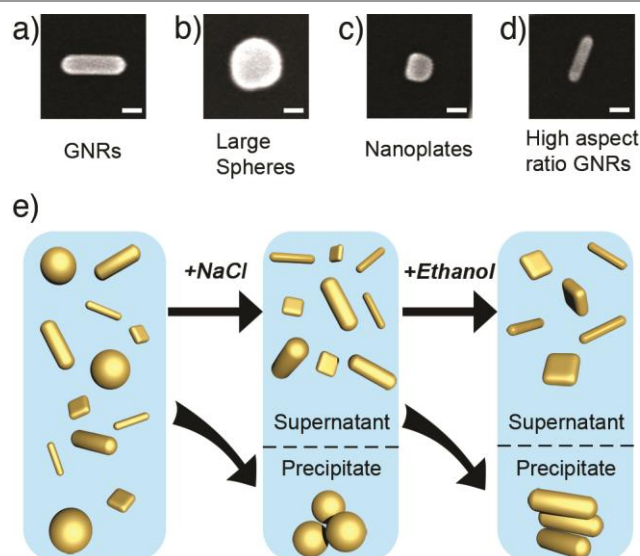


Fig. 1. (a-d) SEM images of a typical GNR with an aspect ratio of 3 (a) and the three nanoparticulate byproducts (b-d). (e) Schematic representation of the GNR purification process following a two-step fractionated precipitation. The scale bar in each image corresponds to 15 nm.

As suggested above, the development of scalable post-synthesis purification methods appears to be crucial to produce stocks of GNR building blocks for the design and fabrication of highly ordered nanoparticle assemblies such as plasmonic waveguides. Several nanoseparation methods have been developed to purify GNR solutions, such as size-exclusion chromatography,²¹ gel electrophoresis,²² centrifugation,²³⁻²⁶ gravitational sedimentation²⁷ and depletion-induced separation.²⁸ Unfortunately these techniques suffer from either low yield and throughput or a poor capacity to fine-tune the separation, especially when the size difference between GNRs and impurities is small. In addition, the majority of these protocols only deal with one type of byproduct, providing only a partial solution to the purification challenge. To our knowledge, only the use of aqueous multiphase systems for rate-zonal centrifugation has the potential to separate more than one species.²⁴

Thiol-PEG-carboxyl (SH-C₁₁H₂₂-(OCH₂CH₂)₆-OCH₂-COOH) modified gold nanoparticles display a sharp size-dependent colloidal stability threshold that can be used for the size-selective separation of nanoparticle solutions.²⁹ The principle is based on the fine balance between the attractive interparticle van der Waals forces driving nanoparticle aggregation and the electrostatic interparticle repulsion that endows nanoparticles with excellent colloidal stability. The resulting electrostatic repulsion forces can easily be attenuated by the ionic strength of the dispersing medium, leading to nanoparticle precipitation beyond specific thresholds of ionic strength. Once precipitated, thiol-PEG-carboxyl functionalized nanoparticles can easily be redispersed in deionized water, making them available for further use.

We have recently shown the conceptual validity of this size-selective colloidal precipitation method by separating nanoparticles from solutions with a bimodal size distribution, consisting of 20 and 40 nm spherical gold nanoparticles with yields beyond 99%.²⁹

The surface functionalization of gold nanoparticles with thiol-PEG-carboxyl presents three advantages: (1) the ligand acts as a nanoparticle stabilizer by conferring negative charges at a neutral pH due to the deprotonated carboxylic groups,²⁰ (2) carboxylic acid-terminated ligands modified GNRs have the ability of advanced self-assembly, they can form two- and three- dimensional superstructures with hexagonal close-packed (hcp) ordering like vertically aligned nanorod arrays^{23,22} and (3) the functionalities present on the ligand make further functionalization simple; for instance via thiol exchange²¹ or crosslinking protocols involving the carboxyl group.²⁴

Herein, we show that size- and shape-selective fractionated precipitation is a convenient strategy to solve complex purification problems such as the separation of GNRs from nanoparticulate side products that inevitably form during their synthesis. Following the surface functionalization of the reaction products with thiol-PEG-carboxyl, we introduce a two-step precipitation protocol to remove byproducts with lower and higher colloidal stabilities than the GNR main product (Fig. 1b). During the first step, the salt concentration of the GNR solution is increased just below the precipitation threshold for the desired GNRs, leading to the precipitation and subsequent removal of particles with less colloidal stability such as the spherical particles shown in Fig. 1b. In the second step, ethanol is added to a concentration just above the critical precipitation threshold of the desired GNRs, leading to their precipitation and leaving smaller more

stable colloidal particles such as high aspect nanorods and nanoplates (Fig. 1c,d) in solution. The precipitated GNRs are separated from the supernatant and can then easily be redispersed in deionized water. In the following we show a detailed analysis of the separation process and its yield. Finally, we use the purified GNRs as building blocks in a self-assembly process to form vertically aligned nanorod arrays and compare the result to the assemblies formed from an unpurified GNR solution.

The separation concept is based on the relationship between the electrostatic interaction energy between colloidal particles and the effective dielectric constant of the dispersing medium. The latter can be conveniently tuned by increasing the ionic strength of the electrolyte and the addition of ethanol. Both lead to a lowering of the dielectric constant,^{25,26} which in turns leads to an increase in interparticle forces and subsequently a reduction in colloidal stability (see Supporting Information).

The gold nanorod synthesis and thiol-PEG- carboxyl modification were performed following previously described procedures (see Supporting Information). For the first size- and shape- selective precipitation step, it is vital to identify the precipitation threshold of the desired GNRs. This is in order to maximize the number of larger impurities that can be precipitated from the reaction solution, while at the same time limiting the unwanted precipitation of desired GNRs. Fig. 2a shows the UV-Vis spectra of the re-dispersed precipitate that formed in NaCl solutions with concentration between 0.3 and 1.8 M over the course of 2 hours. Fig. 2a shows a typical scanning electron microscope (SEM) image of the particles that precipitated from a 1.0 M NaCl solution. It is mainly composed of spherical nanoparticles with an average diameter of 50 nm and a small amount of GNRs. The relevant UV- Vis spectrum shows a strong absorption peak at 535 nm, which is typical for the spherical particles that compose the precipitate.

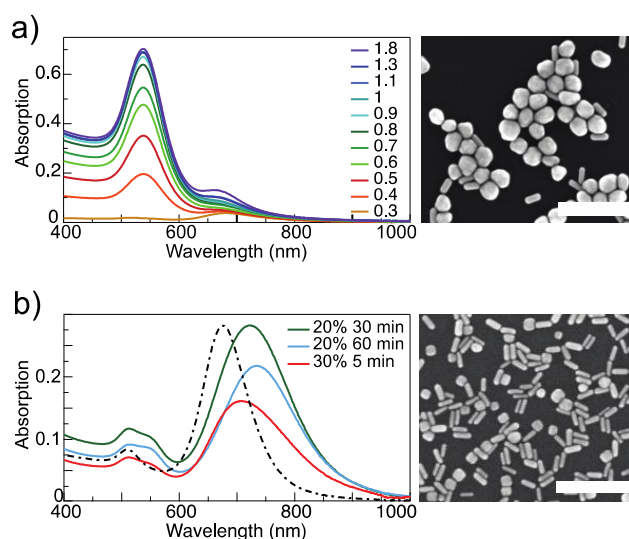


Fig. 2. UV-Vis spectra and associated SEM images of (a) the re-dispersed large spherical nanoparticle byproducts precipitated at different NaCl concentrations (mol/l) during the first nanoseparation and (b) the supernatant containing

nanoplates and high-aspect ratio GNRs following the second nanoseparation with different ethanol concentrations and precipitation times. The dotted line shows a scaled absorption spectrum of the purified GNRs for comparison. The scale bar in each image corresponds to 200 nm. The SEM images show (a) particles that precipitated from a 1.0 M aqueous NaCl solution over the course of 2 hours and (b) particles from the supernatant of a 1.0 M aqueous NaCl solution exposed to 20 vol % for 30 minutes.

It is noteworthy to state that the 535 nm absorption peak is distinct from the transverse plasmon resonance of GNRs at 510 nm (Fig. 4a). The shoulder in the wavelength range of 650-700 nm corresponds to the longitudinal surface plasmon (LSP) resonance of GNRs visible in Fig. 1a. Even at low salt concentrations, this absorption peak is noticeable due to the experimental difficulty to completely remove all supernatant after byproduct precipitation. The absorption peak at 535 nm can be observed for the redispersed precipitate solution for NaCl concentrations of 0.4 M and above. This absorption peak increases with increasing NaCl concentrations, plateauing at a concentration of about 1.0 M (ESI, Fig. S2[†]). This is indicative of a quantitative precipitation of the large spherical impurities at NaCl concentrations of 1.0 M and above. As the NaCl concentration increases, a raise of the absorption peak at 665 nm can be observed, indicative of an increased simultaneous precipitation of GNRs. Since the as-synthesized GNR solution displays a longitudinal absorption at 685 nm and the GNR longitudinal plasmon absorption blue-shifts with decreasing aspect ratio,²⁷ the peak that appears at 665 nm is likely to correspond to the absorption of the lowest aspect ratio GNRs contained in the original GNR solution. The amount of precipitated rods however is still very low. Comparing the GNR absorption of the original GNR solution and the redispersed precipitate reveals that less than about 5 % of rods were removed in this first purification step.

The second purification step aims at separating the GNR main product from the colloiddally more stable impurities such as nanoplates and high-aspect ratio GNRs, shown in Fig. 1c,d. In this purification step, the goal is to precipitate the majority of desirable GNRs, while avoiding the co-precipitation of small impurities in the supernatant to allow for their separation. As shown in the previous section, thiol-PEG-carboxyl modified GNRs show excellent colloidal stability up to salt concentrations of 1.8 M. A convenient strategy to reduce their colloidal stability is to add ethanol.²⁸ Following the exposure of a prepurified GNR solution (dispersed in a 1.0 M NaCl solution) to 20% volume of ethanol, most GNRs precipitated within 30 minutes. Fig. 2b shows the UV-Vis spectra of the supernatant following this second separation process under varying precipitation conditions. In both purification steps, the supernatant is extracted after a short centrifugation of 1 minute to collect the precipitates at the bottom of the Eppendorf tube. The SEM image (Fig. 2b) of particles from the supernatant collected after 30 min exposure to 20% volume of ethanol reveals the presence of nanoplates, high-aspect ratio nanorods, as well as some of the nanorod main product. The nanoplates are identified by a new absorption shoulder peak centered around 555 nm, while the presence of GNRs with different aspect ratios give rise to a red-shifted and broadened LSP resonance peak ($\lambda_{\text{max}} = 725 \text{ nm}$), compared to the purified GNR main product ($\lambda_{\text{max}} = 675 \text{ nm}$). Extending the exposure time from 30 to 60 min results in the precipitation of some of the impurities (nanoplates and high aspect ratio GNRs) that were still contained in the supernatant after 30

minutes. This is witnessed by the reduction of the 555 nm peak and the GNR absorption peak. The difference spectrum derived from the UV/Vis spectra of the supernatant after 30 and 60 min precipitation (ESI, Fig. S4[†]) mainly shows the spectral features of GNRs with an aspect ratio higher than that of the purified GNRs but lower than the GNRs that precipitated during the first 30 min after ethanol addition. A shoulder around 555 nm in the difference spectrum also provides evidence for the precipitation of the undesired nanoplates over this time period. Precipitation at higher ethanol concentration for shorter time also results in an important reduction of the 555 nm peak in the supernatant as well as a reduction and blueshift of the longitudinal plasmon resonance peak, indicating that precipitation at higher ethanol concentrations is less specific in respect to the GNR aspect ratio. Comparing the absorptivity of the GNR solution prior to and after the 2nd purification step indicates a loss of less than 25% in total absorption at 676 nm. This absorption loss is also partially caused by the precipitation of high aspect ratio GNRs, which is desired as it increases the size uniformity of the resulting purified GNR fraction.

A statistical analysis of SEM images was performed to further assess the specificity and yield of the presented separation process at different stages of the purification protocol (Fig. 3a). Electrostatic adsorption was used to immobilize nanoparticles to ensure that the size and shape distribution was representative for the distributions in the according solutions. In brief, a small volume of a dilute nanoparticle solution (6 μL) was pipetted onto an (3-aminopropyl)triethoxysilane (APTES) modified silicon substrate. The substrate was placed in a humidity chamber until completion of the adsorption process (complete discoloration of the solution in 4 hours). We found that as-synthesized GNR solutions (Fig. 3c) contained about 11.4% non-rod-shaped nanoparticles (8.8% nanoplates and 2.6% spherical particles). The first purification process successfully reduced the fraction of spherical nanoparticles to 0.2%. No spherical impurities could be detected in the gold nanorod solution following the complete two-step purification process, while the particle count of nanoplates was reduced to 1.9%, yielding an overall purity of 98.1%. The fraction of spherical particles and nanoplates were estimated for every precipitation condition for both steps (ESI, Fig. S5[†]) based on UV-Vis data (Fig. 2) and statistical analysis (Fig. 3a). The SEM images shown in Fig. 3 provide a representative image of the depletion of the big spherical particles following the first step and the drastic reduction of small impurities after the second step.

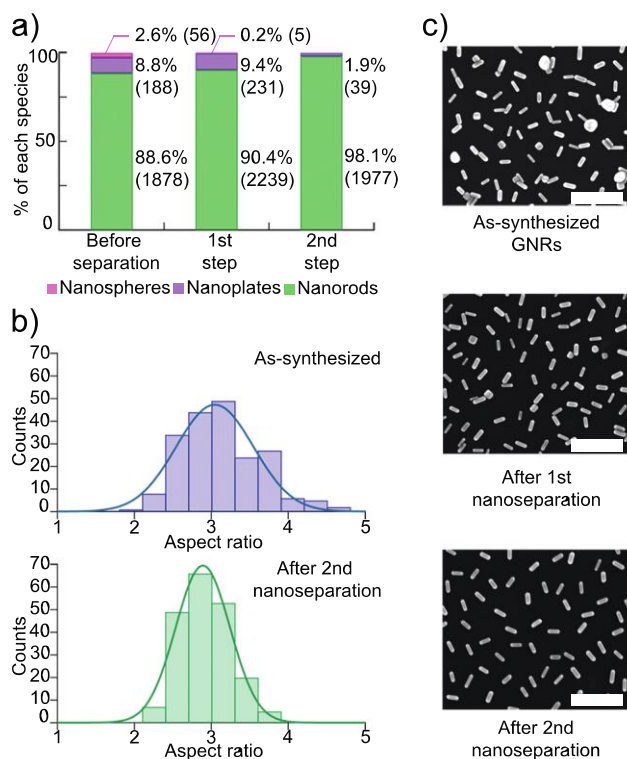


Fig. 3. (a) Statistical analysis of the frequency of occurrence of different nanoparticle species at different stages of the purification process derived from SEM images (particle counts in brackets). (b) GNR aspect ratio distributions of an as-synthesized solution and a purified solution after the second nanoseparation step. (c) SEM images of gold nanoparticles taken at different nanoseparation steps. The scale bar in each image corresponds to 200 nm.

The aspect ratio distributions of as-synthesized and purified GNRs have also been compared (Fig. 3b). The SEM data analysis confirms a significant narrowing of the aspect ratio distribution as a result of the purification process, mostly as a result of the removal of high aspect ratio nanorods. The standard deviation of the aspect ratio between the as-synthesized GNRs and the purified GNRs decreases from 0.5 to 0.3 over the course of the purification process. A comparison of the UV-Vis absorption spectra of the actual GNR solution at the different stages of the purification protocol (Fig. 4a) is in good agreement with the results described above. The removal of large spherical gold nanoparticles and nanoplates is witnessed by a decreased absorption in the 530–560 nm wavelength range and a 5 nm blue-shift. The second purification step significantly alters the actual LSP resonance, leading to a narrowing of the full width at half maximum from 91 nm to 81 nm.

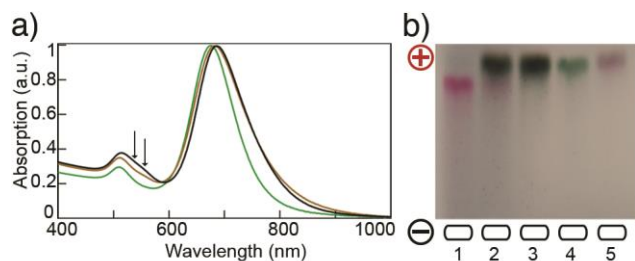


Fig. 4. (a) Normalized UV-Vis spectra of the as-synthesized GNR solution (black), after the first (brown) and second nanoseparation step (green). The consecutive removal of large spherical nanoparticles and nanoplates is reflected by a decrease in absorption around 535 nm (left arrow) and 555 nm (right arrow), respectively. (b) Electrophoretic separation of nanoparticle solutions obtained at different stages of the purification protocol. The different wells contain (1) the re-dispersed precipitate formed during the first nanoseparation, (2) the as-synthesized GNR solution, (3) the supernatant after the first purification step, (4) the re-dispersed purified GNR after the second purification step and (5) the corresponding supernatant.

Sönnichsen and co-workers have shown that gel electrophoresis can be used to separate nanoparticles according to size and shape.²² By mixing gold spherical nanoparticles and GNRs after thiol-PEG-carboxyl functionalization, they observed two colored bands characteristic of each species. Here we use electrophoresis as a simple analytical tool to demonstrate the successful purification of GNR solutions (Fig. 4b). The chromatogram of the as-synthesized GNR solution (well no.2) shows a number of color bands that are not fully separated. The red color band with the highest retention factor can clearly be assigned to the large spherical nanoparticles removed in purification step 1 (well no.1). This band is not visible in the GNR solution following the first purification step (well no.3). The fully purified GNRs gives rise to only one single green color band whereas the impurities removed during the second purification step (well no.5) appear as two overlapping bands with brown and purple color.

To study the effect of GNR purity on the self-assembly behavior, we compared the self-assembly of vertically aligned GNR arrays on a patterned substrate with as-synthesized and purified GNR solutions. This process follows an assembly method that was recently reported by our group.²² It allows the fabrication of confined arrays of standing GNRs characterized by a hexagonal close-packed (hcp) ordering. The template consists of a periodic set of $1 \mu\text{m} \times 3 \mu\text{m}$ gold rectangles on a silica coated silicon wafer with a $3 \mu\text{m}$ edge-to-edge distance. Fig. 5 shows representative SEM images of self-assembled nanostructures made with unpurified (Fig. 5a) and purified nanorods (Fig. 5b). The assembly generated from the purified GNR solution consists almost exclusively of vertically aligned nanorods forming a hexagonal array (ESI, Fig. S9[†]).

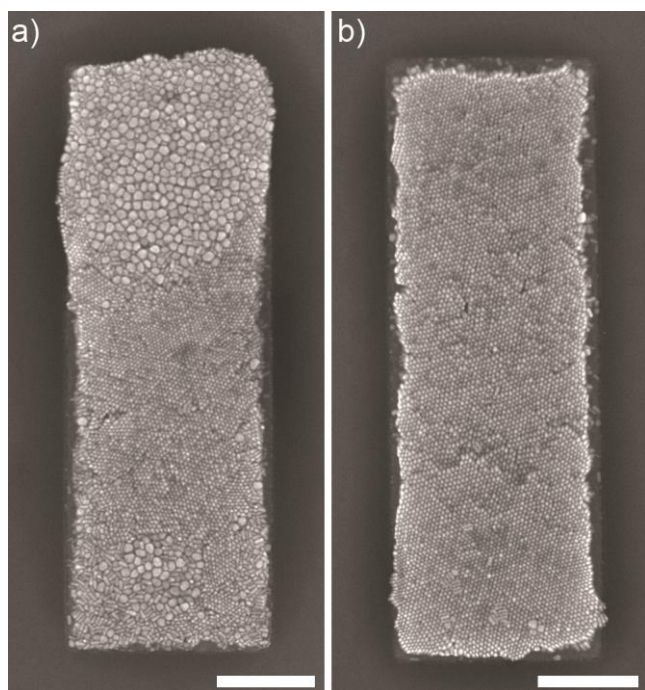


Fig. 5. SEM images of self-assembled vertically aligned GNR arrays in rectangular templates using GNRs from an (a) as-synthesized and (b) purified solutions as building blocks. The scale bar in each image corresponds to 500 nm.

A very small number of defects can be seen where GNRs align perpendicularly to the surface of the substrate. The assembly generated from the unpurified GNRs also shows domains of vertically aligned GNRs. These however are interrupted by domains of large spherical nanoparticles up to about $1 \mu\text{m}^2$ in size. No nanoplates can be observed within the assembly while the larger spherical nanoparticles are statistically overrepresented within the assembly compared to their occurrence in the assembly solution. This is indicative of a shape-selective deposition process,²⁹ favoring the assembly of large spherical nanoparticles over GNRs and nanoplates.

In view of a potential application of GNR arrays as plasmonic waveguides the array self-assembled from the purified GNR solution appears almost defect free whereas the presence of less than 3% of spherical nanoparticles in the building block solution can dramatically disturb the self-assembly process, leading to the formation of large defects within the hcp GNR domain that span across the entire $1 \mu\text{m}$ width of the test structure. These results show the necessity to produce nanoparticulate building blocks with excellent purity and monodispersity if they are to be used for the formation of ordered defect-free self-assembled nanostructures.

In conclusion, we have presented a size- and shape-selective two-step fractionated precipitation method as a convenient strategy to solve a complex purification problem such as the separation of GNRs from nanoparticulate side products formed during their synthesis. Impurities that exhibited higher or lower colloidal stability than the GNR main product were successfully removed, increasing the purity of the as-synthesized GNR solution from 88.6% to 98.1%. The purification process also resulted in a significant narrowing of the aspect-ratio distribution of the GNRs. This fractionated purification method should be universally applicable to a range of nanoparticle

separation problems, to yield shape-uniform monodisperse building blocks in high yield and purity.

The assembly of close to defect-free individual arrays of vertically aligned GNRs was achieved once purified GNR solutions were used for the assembly. The scope of fabricating functional plasmonic metamaterials such as plasmonic waveguides through self-assembly will critically depend on our ability to provide high-grade feedstocks of uniform and pure colloidal building blocks. Simple scalable purification methods such as the two-step fractionated precipitation method presented here will be a welcome tool to prepare nanoparticles of adequate quality for the future assembly of advanced electronic and optical devices.

Acknowledgements

The authors acknowledge financial support from the Australian Research Council through an Australian Research Fellowship (UB). Further financial support has been received from Commonwealth Scientific and Industrial Research Organization through an OCE Science Leader position (UB). This work was performed at the Melbourne Centre for Nanofabrication, an initiative partly funded by the Commonwealth of Australia and the Victorian Government.

Notes and references

^a Department of Materials Engineering, Monash University Wellington Road, Clayton, Victoria 3800, Australia

^b Materials Science and Engineering, Commonwealth Scientific and Industrial Research Organisation Bayview Avenue, Clayton, Victoria 3168, Australia

^c Melbourne Centre for Nanofabrication 151 Wellington Road, Clayton, Victoria 3168, Australia

^d Faculty of Pharmaceutical Sciences, Tokyo University of Science, 2641 Yamazaki, Noda, Chiba 278-8510, Japan

† Electronic Supplementary Information (ESI) available: Materials and Chemicals, Methods and Figures S1-S8 including AFM cross-section analysis, UV-Vis studies and additional SEM images. See DOI: 10.1039/c000000x/

- H. Wang, D. W. Brandl, P. Nordlander, N. J. Halas, *Acc. Chem. Res.* 2007, **40**, 53-62.
- M. A. El-Sayed, *Acc. Chem. Res.* 2001, **34**, 257-264.
- R. Kubo, A. Kawabata, S. Kobayashi, *Annu. Rev. Mater. Sci.* 1984, **14**, 49-66.
- D. Solis, B. Willingham, S. L. Nauert, L. S. Slaughter, J. Olson, P. Swanglap, A. Paul, W.-S. Chang, S. Link, *Nano Lett.* 2012, **12**, 1349-1353.
- G. A. Wurtz, W. Dickson, D. O'Connor, R. Atkinson, W. Hendren, P. Evans, R. Pollard, A. V. Zayats, *Opt. Express* 2008, **16**, 7460-7470.
- M. Février, P. Gogol, A. Aassime, R. Mégy, C. Delacour, A. Chelnokov, A. Apuzzo, S. Blaize, J.-M. Lourtioz, B. Dagens, *Nano Lett.* 2012, **12**, 1032-1037.
- X. Huang, S. Neretina, M. A. El-Sayed, *Adv. Mater.* 2009, **21**, 4880-4910.

- 8 P. K. Jain, S. Eustis; M. A. El-Sayed, *J. Phys. Chem. B* 2006, **110**, 18243-18253.
- 9 A. M. Funston, C. Novo, T. J. Davis, P. Mulvaney, *Nano Lett.* 2009, **9**, 1651-1658.
- 10 B. Nikoobakht, M. A. El-Sayed, *Chem. Mater.* 2003, **15**, 1957-1962.
- 11 G.-T. Wei, F.-K. Liu, C. R. Chris Wang, *Anal. Chem.* 1999, **71**, 2085-2091.
- 12 M. Hanauer, S. Pierrat, I. Zins, A. Lotz, C. Sönnichsen, *Nano Lett.* 2007, **7**, 2881-2885.
- 13 V. Sharma, K. Park, M. Srinivasarao, *Proc. Natl. Acad. Sci. U.S.A.* 2009, **106**, 4981- 4985.
- 14 O. Akbulut, C. R. Mace, R. V. Martinez, A. A. Kumar, Z. Nie, M. R. Patton, G. M. Whitesides, *Nano Lett.* 2012, **12**, 4060-4064.
- 15 X. Ma, Y. Kuang, L. Bai, Z. Chang, F. Wang, X. Sun, D. G. Evans, *ACS Nano* 2011, **5**, 3242-3249
- 16 W. Peng, R. Mahfouz, J. Pan, Y. Hou, P. M. Beaujuge, O. M. Bakr, *Nanoscale*, **5**, 5017-5026
- 17 B. P. Khanal, E. R. Zubarev, *J. Am. Chem. Soc.* 2008, **130**, 12634-12635.
- 18 K. Park, H. Koerner, R. A. Vaia, *Nano Lett.* 2010, **10**, 1433-1439.
- 19 Y. Zheng, C. H. Lalander, U. Bach, *Chem. Commun.* 2010, **46**, 7963-7965.
- 20 M. R. Jones, R. J. Macfarlane, A. E. Prigodich, P. C. Patel, C. A. Mirkin, *J. Am. Chem. Soc.* 2011, **133**, 18865-18869.
- 21 C. Hamon, M. Postic, E. Mazari, T. Bizien, C. Dupuis, P. Even-Hernandez, A. Jimenez, L. Courbin, C. Gosse, F. Artzner, V. Marchi-Artzner, *ACS Nano* 2012, **6**, 4137-4146.
- 22 T. Thai, Y. Zheng, S. H. Ng, S. Mudie, M. Altissimo, U. Bach, *Angew. Chem., Int. Ed.* 2012, **51**, 8732-8735.
- 23 S. Perumal, A. Hofmann, N. Scholz, E. Rühl, C. Graf, *Langmuir* 2011, **27**, 4456-4464.
- 24 A. Salvati, A. S. Pitek, M. P. Monopoli, K. Prapainop, F. Baldelli Bombelli, D. R. Hristov, P. M. Kelly, C. Åberg, E. Mahon, K. A. Dawson, *Nat. Nanotechnol.* 2013, **8**, 137- 143.
- 25 R. Buchner, G. T Hefter, P. M. May, *J. Phys. Chem. A*, 1999, **103**, 1-9
- 26 G. Akerlof, *J. Am. Chem. Soc.*, 1932, **54**, 4125-4139
- 27 S. W. Prescott, P. Mulvaney, *J. Appl. Phys.* 2006, **99**, 123504.
- 28 J. Liao, Y. Zhang, W. Yu, L. Xu, C. Ge, J. Liu, N. Gu, *Colloids Surf., A* 2003, **223**, 177-183.
- 29 Z. Xu, C. Shen, C. Xiao, T. Yang, S. Chen, H. Li, H. Gao, *Chem. Phys. Lett.* 2006, **432**, 222-225.